

Automatic Detection of Rib Borders in Chest Radiographs

Zhanjun Yue, Ardeshir Goshtasby, *Senior Member, IEEE*, and Laurens V. Ackerman, *Member, IEEE*

Abstract—An algorithm for detection of posterior rib borders in chest radiographs is presented. The algorithm first determines the thoracic cage boundary to restrict the area of search for the ribs. It then finds approximate rib borders using a knowledge-based Hough transform. Finally, the algorithm localizes the rib borders using an active contour model. Results of the proposed rib finding algorithm on 10 chest radiographs are presented.

I. INTRODUCTION

CHEST radiographs remain the initial and often the most valuable means for investigating the chest. They are an indispensable part of the physical examination which precedes many operations, and provide evidence to solve many medical diagnostic problems. Pulmonary disease, cardiovascular pathology, and skeletal lesions can be studied using chest radiographs [1], [2].

Chest radiographs provide the radiologist with information about several different organ systems: cardiovascular, respiratory, and skeletal. Within the latter group, ribs, spine, scapula, proximal humeri, and shoulder joints are included. This "mini skeletal survey" can provide a wealth of information about the patient. Areas of bone destruction may be signs of cancer [3], [4] or, in the case of a missing rib, a prior surgical procedure in the thorax. Dense or sclerotic ribs may also be a sign of cancer but may indicate sickle cell disease, endstage renal disease, or other metabolic disease. Rib fractures have several different "tales to tell." When associated with a traumatic event, they cause the radiologist to search for other signs of chest injury: pneumothorax, hemothorax, lung contusion, or tear of the aorta. If the fractures are not associated with trauma, they may signal an underlying cancer (the "pathologic" fracture), osteoporosis, or even osteomalacia. In children, multiple fractured ribs of different ages raise the question of child abuse. Deformed, or incompletely formed ribs may be the sign of rickets or neurofibromatosis. Notched ribs are associated with coarctation of the aorta.

Automatic analysis of chest radiographs can improve health care by eliminating user bias and reducing radiologists' efforts in the analysis [5], [6]. Ribs provide a convenient frame of reference in the chest and make it possible to locate organs such as the heart, lung, and vertebral bodies [7].

Manuscript received November 25, 1993; revised May 10, 1995. The Associate Editor responsible for coordinating the review of this paper and recommending its publication was J. S. Duncan.

Z. Yue and A. Goshtasby are with the Department of Electrical Engineering and Computer Science, University of Illinois, Chicago, IL 60607-7053 USA; e-mail: yue@bert.eecs.uic.edu.

L. V. Ackerman is with the Department of Diagnostic Radiology and Nuclear Medicine, Rush-Presbyterian-St. Luke's Medical Center, Chicago, IL 60607 USA.

IEEE Log Number 9413558.

One of the first attempts to detect ribs automatically was made by Toriwaki *et al.* [8], assuming that all ribs had the same width and were equally spaced. Using preselected areas in a chest radiograph, Persoon *et al.* [9] located rib borders by template matching. Wechsler [6] developed an algorithm that could detect rib borders using a heuristic method that searched for parabolic segments. Kulick *et al.* [10], Li *et al.* [11], and Souza [12] took vertical sections through the lung and determined rib edge points. Rib borders were then determined by fitting curves to the edge points.

In this paper, an automatic method for detection of posterior rib borders is presented. The method first isolates the area of search for the ribs by extracting the thoracic cage boundary. It then searches for the ribs in the thoracic cage using a knowledge-based Hough transform.

A rib border will be represented by two parabolic segments. The parabolic segments will be replaced by an active contour model later to localize the rib border. An active contour adapts to the local shape of a rib border by continuously minimizing its energy. Active contours provide information about the local shape of ribs and are, therefore, valuable in detecting and evaluating rib abnormalities in chest radiographs.

The posteroanterior (PA) view of the chest is the view most often used in diagnosis. It is obtained by placing the patient's chest against X-ray film and directing the X-ray beam toward the patient's back. This view is known to give the most undistorted view of the heart and chest [1, p. 39].

Given a PA chest radiograph, our goal is to detect and localize the posterior rib borders. As is often the case, ribs near the top of the lung and below the diaphragm are hardly visible and difficult to identify. The first rib is occluded by the second rib, and the eleventh and twelfth ribs are almost completely hidden by the shadow of the abdomen. We will not detect these ribs. The remaining eight ribs, the second through the tenth, will be detected. Due to the symmetry of the chest, the algorithm will be described only for the left half of the chest. Ribs in the right half can be determined similarly.

The proposed algorithm is based on the following assumptions:

- 1) The input will be a standard PA chest radiograph containing the entire thorax with the spinal column appearing vertical. The proposed algorithm is not invariant of the orientation of a chest radiograph, and therefore, if the spinal column is nonvertical, a preprocessing operation is required that will rotate the image to bring the spinal column into the vertical orientation.
- 2) The radiograph should show the two lungs as bright regions and the midthoracic vertebral bodies as a dark

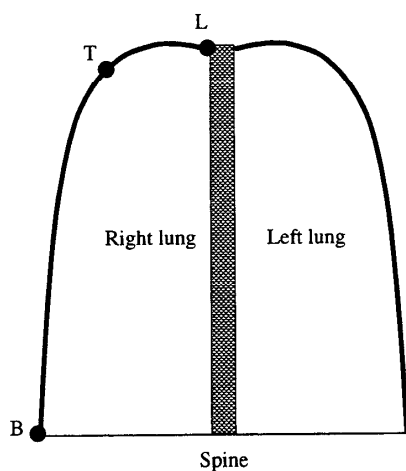


Fig. 1. A thoracic cage boundary, defined by segments LT and TB .

region. This assumption serves to distinguish negative from positive radiographs.

The remainder of this paper is organized as follows: Section II discusses extraction of the thoracic cage. Section III outlines detection of the approximate rib borders. Section IV discusses localization of the rib borders, and subsequent sections present the experimental results, discussion, and conclusions.

II. EXTRACTION OF THE THORACIC CAGE

The thoracic cage boundary delimits the area of search for the ribs. While Ballard [5] used the lung as the area of search for ribs, Fu *et al.* [13] extracted five key points on the lung boundary and used the enclosing area as the search area. Souza [12] traced the outer edge of the lung by a moving window to determine the thoracic cage. Souza's process, however, did not know when to stop, and obtained lung boundaries often extended to the top or the bottom of the radiograph. All of these methods used preselected areas in a chest radiograph to restrict the search area for the ribs. The algorithm presented here does not look in prespecified areas in an image and thus is invariant of the position of the thorax in a chest radiograph.

The thoracic cage boundary is the projection of the lateral ribs onto a 2-D plane. This projection forms a dark ribbon along the outer edge of the lung. In this work, the thoracic cage boundary is defined as a curve that follows the top and lateral borders of the thorax, as shown in Fig. 1. The thoracic cage boundary of the right lung is shown by curve LTB .

Since ribs are confined in the thoracic cage, the thoracic cage provides useful information about the positions of ribs in a chest radiograph. We will extract the thoracic cage by finding two segments, LT and TB , as shown in Fig. 1. We begin by extracting a set of image features from the horizontal and vertical signatures of the image. Based on these features, we will locate the lower part, TB , by dynamic programming. Then we will determine the upper part, LT , by fitting a quadratic curve to pixels within a prespecified ribbon on top of the lung.

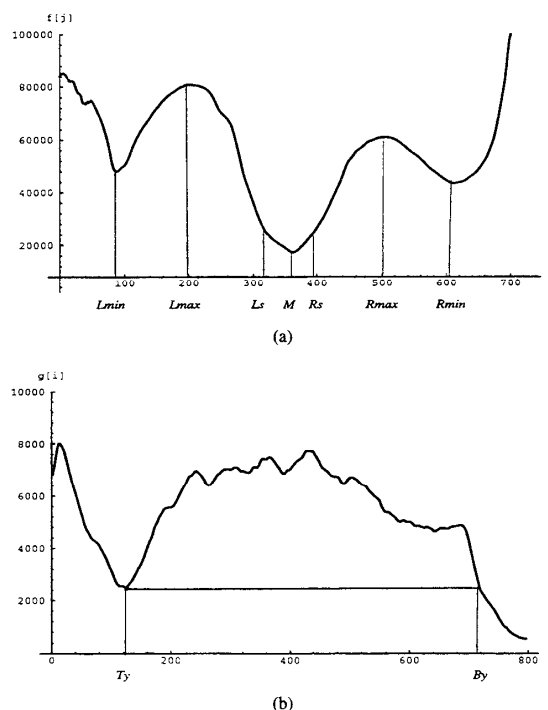


Fig. 2. (a) A horizontal signature. (b) A vertical signature.

A. Image Features Used to Extract the Thoracic Cage

Several image features determined from the horizontal and vertical signatures of the chest image will be used to extract the thoracic cage. Let $I[i, j]$ denote the intensity of pixel at (i, j) , where $0 \leq i \leq N_r - 1$, $0 \leq j \leq N_c - 1$. N_r is the number of rows and N_c is the number of columns in the image. The horizontal signature, denoted by $f[j]$, is defined by

$$f[j] = \sum_{i=0}^{N_r-1} I[i, j], \quad j = 0, \dots, N_c - 1. \quad (1)$$

To prevent the signature from having noisy peaks, it is smoothed with a five-point averaging operator: $[1, 1, 1, 1, 1]/5$. The operator is relatively small and will not change the locations of important features in the signature. One typical horizontal signature is shown in Fig. 2(a) with seven feature points

L_{\min} : a minimum representing the right boundary of the thoracic cage,

L_{\max} : a maximum representing the middle of the right lung,

M : a minimum representing the center of the spinal column,

R_{\max} : a maximum representing the middle of the left lung,

R_{\min} : a minimum representing the left boundary of the thoracic cage,

L_s : location of the right edge of the spinal column,

R_s : location of the left edge of the spinal column.

The edge locations of the spinal column, L_s and R_s , are estimated from

$$\begin{aligned} L_s &= M - (R_{\min} - L_{\min})/12 \\ R_s &= M + (R_{\min} - L_{\min})/12. \end{aligned} \quad (2)$$

This is based on the observation that in most chest radiographs, the vertebral column has a width of approximately one-sixth of the average width of the thorax and is symmetric about the center line M . These parameters are used to define the search area where ribs should be searched. For instance, variations in estimation of L_s and R_s will make detected rib borders slightly longer or shorter at the end extending to the spinal column.

The vertical signature, denoted by $g[i]$, is obtained from a vertical ribbon of width w centered at column L_{\max} where the ribs are most clearly seen

$$g[i] = \sum_{j=L_{\max}-w}^{L_{\max}+w} I[i, j], \quad i = 0, \dots, N_r - 1. \quad (3)$$

In this study, $W = (L_s - L_{\min})/8$ was assumed. A typical vertical signature is shown in Fig. 2(b) with two feature points

T_y : vertical position representing the top of the lung,
 B_y : approximate bottom edge of the lung, obtained such that $g[B_y] = g[T_y]$.

The vertical positions of points T and B in Fig. 1 are then set equal to T_y and B_y , respectively. Parameters L_s and R_s are refined using the horizontal signature of the image between rows T_y and B_y .

B. Locating the Lower Part of the Thoracic Cage by Dynamic Programming

Because the lateral ribs are perpendicular to the X-ray film, they form a dark and narrow ribbon along the lung border. Thus, the intensities of the pixels on the thoracic cage boundary are among the smallest in an image, except for pixels corresponding to the vertebral bodies. We will locate the lower part of the thoracic cage by finding the minimum cost path between rows T_y and B_y . The cost is measured in terms of pixel intensities.

Let x_i , $1 \leq i \leq n$, denote the column position of the minimum path in row $T_y + i - 1$, and n be the total number of rows between T_y and B_y , that is, $n = B_y - T_y + 1$. We will then minimize the cost function

$$\begin{aligned} h(x_1, x_2, \dots, x_n) &= \sum_{i=2}^{n-1} I[T_y + i - 1, x_i] \\ &+ \frac{1}{2} I[T_y, x_1] + \frac{1}{2} I[B_y, x_n]. \end{aligned} \quad (4)$$

$I[T_y + i - 1, x_i]$ denotes the pixel value at row $T_y + i - 1$ and column x_i . $h(x_1, x_2, \dots, x_n)$ represents the sum of all pixel intensities between rows $T_y + 1$ and $B_y - 1$ and half of pixel intensities at rows T_y and B_y . Determining the minimum of h by brute force requires exhaustive enumeration of all combinations of x_1, \dots, x_n , which is computationally prohibitive. Using dynamic programming [14, p. 137], we will

decompose the problem into a number of small steps and then solve the problem step by step. Rewriting our cost function by

$$\begin{aligned} h(x_1, \dots, x_n) &= h_1(x_1, x_2) + h_2(x_2, x_3) \\ &+ \dots + h_{n-1}(x_{n-1}, x_n), \end{aligned} \quad (5)$$

we can let $h_i(x_i, x_{i+1})$ represent half the sum of pixel intensities at x_i and x_{i+1}

$$h_i(x_i, x_{i+1}) = \frac{1}{2} \{I[T_y + i - 1, x_i] + I[T_y + i, x_{i+1}]\}. \quad (6)$$

In order to obtain a continuous thoracic cage boundary, we require neighboring pixels on the minimum cost path be connected, that is, $|x_i - x_{i+1}| \leq 1$. Denoting the smallest value of h_1 for different values of x_2 by $f(2, x_2)$, we have

$$f(2, x_2) = \min\{h_1(x_1, x_2) : x_1 = x_2 - 1, x_2, x_2 + 1\}. \quad (7)$$

The smallest value of $h_1(x_1, x_2)$ is now a function of only one variable, x_2 . Further, x_2 can be eliminated by computing the smallest value, denoted by $f(3, x_3)$, for different values of x_3

$$\begin{aligned} f(3, x_3) &= \min\{f(2, x_2) + h_2(x_2, x_3) : \\ &x_2 = x_3 - 1, x_3, x_3 + 1\}. \end{aligned} \quad (8)$$

This smallest value is now only a function of x_3 . In general, we can write

$$\begin{aligned} f(i, x_i) &= \min\{f(i-1, x_{i-1}) + h_{i-1}(x_{i-1}, x_i) : \\ &x_{i-1} = x_i - 1, x_i, x_i + 1\}, \quad 2 < i < n. \end{aligned} \quad (9)$$

Therefore, to obtain the thoracic cage boundary, we initialize $f(1, j) = \frac{1}{2} I[T_y, j]$ and compute

$$\begin{aligned} f(i, j) &= I[i, j] + \min\{f(i-1, j-1), f(i-1, j), \\ &f(i-1, j+1)\} \end{aligned} \quad (10)$$

for $T_y + 1 \leq i \leq B_y - 1$. Finally, we determine

$$\begin{aligned} f(n, j) &= \frac{1}{2} I[B_y, j] + \min\{f(n-1, j-1), f(n-1, j), \\ &f(n-1, j+1)\}. \end{aligned} \quad (11)$$

j is allowed to vary between 1 and L_{\max} . $f(i, j)$ is thus the minimum cost between pixel $(T_y + i - 1, j)$ and row B_y . When determining the minimum value of $\{(i-1, j-1), (i-1, j), (i-1, j+1)\}$, we set up a pointer from pixel $(T_y + i, j)$ to the pixel with the minimum cost in its neighborhood in row $T_y + i - 1$. The cost of the minimum path is the smallest of $f(B_y, j)$ for $1 \leq j \leq L_{\max}$. As a result of this computation, contour segment TB is obtained. Note that although j is allowed to change from column 1 to column L_{\max} , in practice, it stays in the small neighborhood of column L_{\min} .

C. Determining the Upper Part of the Thoracic Cage by Curve Fitting

At the top of the lung, the image becomes more complex and dynamic programming cannot find the thoracic cage. Because of its parabolic shape, we will find the upper part of the thoracic cage by fitting a quadratic polynomial to pixels in a parabolic support region. A parabola defined by

$$y = a(x - d)^2 + c \quad (12)$$

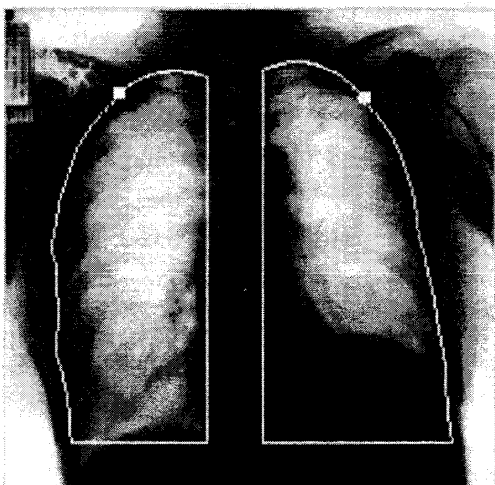


Fig. 3. Extracted thoracic cage boundaries in a chest radiograph.

will be used to represent the upper part of the thoracic cage, where the y -axis is vertical, the x -axis is horizontal, and the origin is at the upper-left corner of the image. We define a support region by substituting $d = L_s$, and letting

$$\begin{cases} 0.001 \leq a \leq 0.01 \\ L_{\min} \leq c \leq y_t \end{cases} \quad (13)$$

in relation to (12). y_t is the y -coordinate of point T on the thoracic cage. Range of values for parameter a was experimentally determined by manually tracing along the upper part of the rib cage in many chest radiographs and determining parameter a of parabolas fitting the obtained contours. Parameter c was allowed to assume all possible values. A parabolic curve was then fitted to edge points representing locally maximum gradient magnitudes [15] in the obtained support region and minimizing

$$E = \sum_{i=1}^N m_i \{y_i - [a(x_i - d)^2 + c]\}^2 \quad (14)$$

where

- E is the objective function to be minimized,
- N is the total number of pixels with locally-maximum gradient magnitudes in the region,
- i indicates the i th pixel in the region,
- m_i is the gradient magnitude of pixel i ,
- x_i and y_i are the coordinates of pixel i ,
- a , d and c are the parameters to be determined.

Fig. 3 shows the thoracic cage boundary extracted in a chest radiograph. The small squares show places where the upper and lower parts of the boundary join. Due to image noise, the upper and lower cage boundaries obtained by the above procedures may not coincide. Our program will connect the end points of the upper and lower boundaries if they are not already connected.

III. DETECTION OF RIB BORDERS

Chest radiographs contain noise and occlusion inherent in X-ray photography. Optical intensities across a rib change considerably, and in some instances, parts of a rib boundary disappear. Hough transform has been recognized as a technique for detecting analytically defined shapes or predefined templates in an image. Although Hough transform has been studied extensively [16]–[19], its use in practice has been limited. In the following, we will point out difficulties associated with the use of Hough transform and suggest strategies to overcome them when estimating the rib parameters in a chest radiograph.

A. Hough Transform

Hough transform (HT) was first introduced as a method for detecting sparse straight lines in binary images [20]. It was then found to be a special case of a more general transform, the Radon transform in 2-D [21]. Letting $F(x, y)$ be an arbitrary function defined on plane D , the Radon transform of $F(x, y)$, denoted by $f(\theta, \rho)$, is given by

$$f(\theta, \rho) = \iint_D F(x, y) \delta(\rho - x \cos \theta - y \sin \theta) dx dy \quad (15)$$

where θ and ρ are the polar coordinates of a line, and δ is the Dirac delta function. The space formed by parameters θ and ρ is called the parameter space or the *Hough space*.

The generalization from line detection to curve detection is straightforward. Let

$$\rho = C(x, y; a_1, \dots, a_n) \quad (16)$$

be the equation for some family of curves in the xy plane parameterized by n parameters a_1, \dots, a_n . The generalization of transform (15) for curve detection is given by

$$f(a_1, \dots, a_n) = \iint_D F(x, y) \delta[\rho - C(x, y; a_1, \dots, a_n)] dx dy. \quad (17)$$

This shows that image points on a curve characterized by a_1, \dots, a_n will map to hypersurfaces in the n -dimensional Hough space, and a point in Hough space will map to a curve in the image space. The parameters of a curve are estimated by determining the point in Hough space which is produced from the largest number of intersections of the hypersurfaces.

B. Difficulties in Estimation of the Hough Parameters

Although HT seems an important tool in computer vision, it has problems which prevent it from being used universally. The principal problem with HT is its high computational and memory requirements. Determination of n parameters, each quantized into α intervals, requires an accumulator array of size α^n elements. This can be prohibitively large if either α or n is large. Most applications of HT detect straight lines which require determination of only two parameters [16]. Rib borders are not straight lines, therefore they require determination of at least three parameters. Increasing the Hough space by one

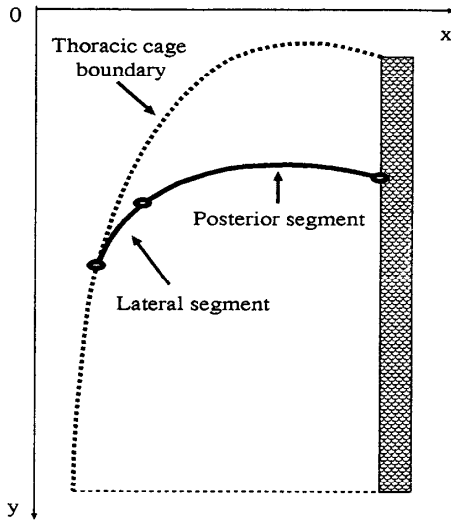


Fig. 4. A rib model consisting of two parabolic segments.

dimension will drastically increase the memory requirements and computation time.

The second problem with HT is its low accuracy in detecting boundaries of natural objects. Almost all applications of HT have been concerned with the detection of boundaries of man-made objects: straight lines, circles, and ellipses [19]. The image curves to be detected have been represented by analytical formulas, and the intersections of hypersurfaces mapped from image points have generally fallen in a small neighborhood in the Hough space, allowing detection of the curves. The rib borders, however, do not map to exact mathematical formulas. If a mathematical curve is used to approximate a rib border, the intersections of hypersurfaces obtained from image points will not fall in a small neighborhood. Furthermore, because of the large number of irrelevant edge pixels and sparsity of edge pixels, detection of clusters in the Hough space becomes difficult.

Another problem associated with HT is its inability to determine the extent of an image curve. It can indicate the possible presence of an image curve, but it embodies no notion of curve termination points. For example, if a partial circle exists in the image, HT cannot tell whether it is a complete or a partial one.

Finally, HT alone cannot determine true object boundaries. The local peaks in the Hough space can only provide candidates for object boundaries. A high level reasoning process is needed to determine whether these candidates truly represent object boundaries in an image.

C. Design of a Knowledge-Based HT for Extraction of the Rib Borders

The rib detection algorithm described in this paper functions in two ways: 1) it uses a rib model to extract candidate rib borders by the HT, and 2) it uses rule-based reasoning to select true rib borders from among the candidates.

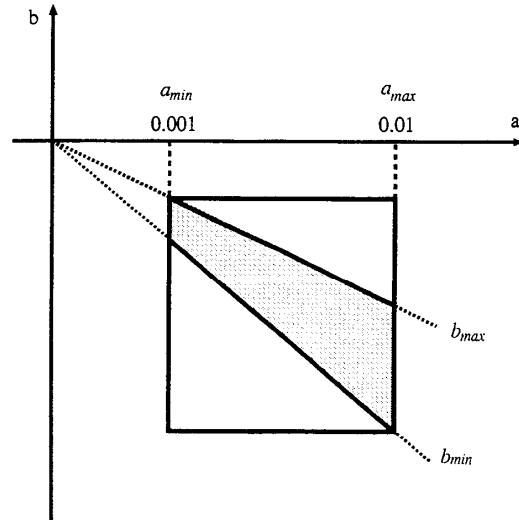


Fig. 5. Reduced search area (shown by the shaded polygon) in the Hough space.

The rib model used in this paper contains two segments: the *posterior* and the *lateral* segments, as shown in Fig. 4. The posterior segment is described by a parabola of the form

$$y = a(x - x_c)^2 + b(x - x_c) + y_c \quad (18)$$

where (x_c, y_c) represents the right endpoint of the segment which is allowed to slide along the left edge of the spinal column. In (18), a , b , and y_c are variables, while $x_c = L_s$ (Fig. 2(a)).

The lateral segment is modeled by a parabola of the form

$$x = v(y - y_0)^2 + x_0 \quad (19)$$

where point (x_0, y_0) is allowed to slide along the thoracic cage boundary. Ranges of the parameters for the model ribs are experimentally determined by manually tracing the rib borders and fitting parabolas to them. Using the rib models, we resolve the problems associated with HT as follows:

- 1) Computation time is reduced by restricting the search area of the Hough space. This is accomplished using the allowable range of parameters of the rib models. For example, to detect the posterior segments, only the shaded area shown in Fig. 5 needs to be explored

$$0.001 \leq a \leq 0.01$$

$$-2a(4W_r + L_s) \leq b \leq 2a(4W_r - L_s) \quad (20)$$

where W_r is the estimated rib width, and L_s is the left edge position of the spinal column shown in Fig. 2(a). W_r was set to $(B_y - T_y)/20$ because there are 10 ribs between T_y and B_y and the distance between two adjacent ribs is about the same as the width of a rib.

- 2) Detection accuracy is increased by using only the *constructive image points*. Constructive image points are high gradient pixels that could possibly contribute to the final curve. Fig. 6(a) and (b) shows the constructive



Fig. 6. High-gradient pixels used to detect (a) the posterior and (b) the lateral rib segments.

edge pixels of gradients ≥ 5 for detecting the posterior and lateral rib segments. Only edges in Fig. 6(a) are used to detect the posterior segments and only edges in Fig. 6(b) are used to detect the lateral segments. The width of the lateral region is taken to be 1/5th and the width of the posterior region is taken to be 4/5th of the horizontal distance between the thoracic cage boundary and the spinal column.

- 3) The endpoints of a curve are obtained from its intersections with the border of the constructive image region. The endpoints of a posterior segment are set to the left and right borders of the region shown in Fig. 6(a), and the endpoints of the lateral segments are set to the thoracic cage boundary and the right border of the region shown in Fig. 6(b).
- 4) Knowledge is incorporated into the extraction process for true rib borders. The parabolic segments represented by the local peaks in the Hough space are used as candidate rib borders. Using rule-based reasoning, true rib borders are then selected from among the candidate ones. The rules are based on the anatomic knowledge of the chest (described later).

The proposed algorithm first detects image edges in the thoracic cage using the conventional edge detectors. From the edge pixels, constructive edge pixels of both the posterior and lateral rib segments are selected. For each constructive edge pixel, a plane is drawn in the parameter space. The accumulator array cells that fall on the plane are incremented by the gradient magnitude of the edge pixel. In the next step, local peak array cells are used to determine the candidate rib borders.

Search for the local peaks in the 3-D accumulator array is expensive and turns out to be unnecessary. Since the ribs

intersect the spinal column, we need only detect the local peaks in the vertical direction. We accomplish this by projecting the maxima of the 3-D accumulator array onto the y -axis. Let $V[a, b, y_c]$ represent the 3-D accumulator array used to represent the Hough space. Then, its 1-D projection, denoted by $K[y_c]$, is obtained from

$$K[y_c] = \max\{V[a, b, y_c] : a \in [a_{\min}, a_{\max}], b \in [b_{\min}, b_{\max}]\}. \quad (21)$$

$K[y_c]$ shows the most probable rib borders which start from vertical position y_c . Along with each y_c , parameters a and b , which are needed to reconstruct a rib, are also saved. The local peaks are selected by comparing the values of three adjacent pixels.

Once the local peaks are obtained, they are taken as candidate rib borders. True rib borders are then selected from these candidates using rule-based reasoning. The goal of the rule-based reasoning is to find pairs of candidate superior and inferior rib borders that represent true ribs in a chest radiograph. Specifically, if $\{U_1, \dots, U_p\}$ denote candidate superior rib borders and $\{L_1, \dots, L_q\}$ denote candidate inferior rib borders, we extract nine ribs—ribs two through ten—each with a superior and inferior border. If we represent each rib by (U_{m_i}, L_{n_i}) , where i shows the rib number, then the nine ribs can be denoted by

$$\{(U_{m_2}, L_{n_2}), \dots, (U_{m_{10}}, L_{n_{10}})\} \quad (22)$$

where $1 \leq m_i \leq p$ for $2 \leq i \leq 10$, and $1 \leq n_j \leq q$ for $2 \leq j \leq 10$.

To determine the relationship between ribs, we use features from each pair of superior and inferior ribs. Let us denote a superior segment by

$$U_i = (a_u, b_u, y_{cu}, x_{us}, y_{us}, x_{ue}, y_{ue}, v_u)_i, \quad 1 \leq i \leq p \quad (23)$$

and an inferior rib by

$$L_j = (a_l, b_l, y_{cl}, x_{ls}, y_{ls}, x_{le}, y_{le}, v_l)_j, \quad 1 \leq j \leq q \quad (24)$$

where a_u , b_u , and y_{cu} are the variable parameters in (18), x_{us} , y_{us} , x_{ue} , y_{ue} are the x and y coordinates of the left and right ends of the superior segment, and v_u is the count in the accumulator array. The parameters in the inferior segment L_j have similar meanings. The features that are used to characterize a pair (U_i, L_j) are:

1) D_s^{ij} : The width of the pair at the left endpoint. It is defined as the distance from the left endpoint, (x_{us}, y_{us}) shown in Fig. 7, of the superior segment U_i to the inferior segment L_j (or vice versa if the superior segment happens to be longer than the inferior one). This measure is used to reject pairs with unreasonably large or small widths at the left end.

2) D_e^{ij} : The width of the pair at the right endpoint. It is defined as the perpendicular distance from the right endpoint (x_{ue}, y_{ue}) of U_i to L_j . This feature is good for rejecting pairs with unreasonably large or small widths at the right end.

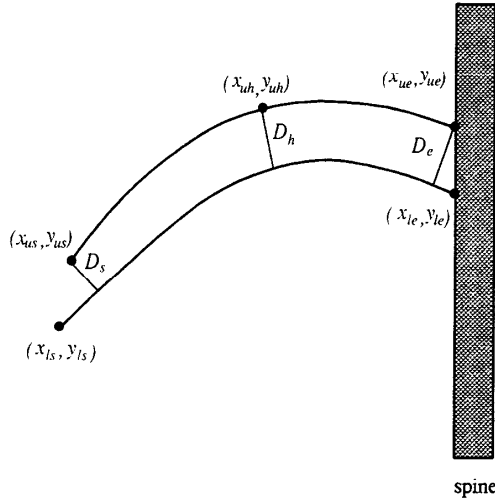


Fig. 7. Distance measures computed from detected rib borders.

3) D_h^{ij} : The width of the pair in the middle of the rib. It is defined as the distance from the middle point (x_{uh}, y_{uh}) on U_i , where $x_{uh} = (x_{us} + x_{ue})/2$, to the inferior segment L_j . Since parabolas are defined by three parameters, the previous two distance measures cannot determine whether two parabolic segments are within a required distance of each other. This distance measure ensures that the middle parts of the superior and inferior segments are also within a required distance of each other.

4) D_r^{ij} : The standard deviation of distances from all points on the superior segment U_i that have correspondences on the inferior segment L_j . This measure is defined by

$$D_r^{ij} = \frac{1}{N_u} \sum_{m=1}^{N_u} \sqrt{[d_{ij}(x_m, y_m) - D_v^{ij}]^2} \quad (25)$$

where $d_{ij}(x_m, y_m)$ is the distance from a point (x_m, y_m) on the superior segment U_i to the inferior segment L_j , and

$$D_v^{ij} = \frac{1}{N_u} \sum_{m=1}^{N_u} d_{ij}(x_m, y_m) \quad (26)$$

is the average distance of the superior and inferior rib borders. N_u is the number of pixels on U_i whose correspondences exist on L_j . Feature D_r^{ij} measures the degree of parallelism of the two parabolic segments.

5) F^{ij} : The confidence level of the pair. It is defined by

$$F^{ij} = \frac{v_u + v_l}{D_r^{ij}} \quad (27)$$

where v_u and v_l are counts of rib segments U_i and L_j in the Hough space, respectively. This feature is used to determine the pair that is most likely to be a true rib when several pairs intersect with one another. The pair with the highest confidence level is retained while others are rejected. This tends to make the retained pairs have higher counts and greater parallelism than other pairs.

The rule-based system consists of the following three components:

- a database of information (containing the obtained parabolic segments),
- a set of rules that modify the database, and
- a control mechanism that determines the selection of the rules.

Initially, the database holds the candidate segments. Candidate pairs which are riblike are added to the database. The candidate pairs are then compared with each other and implausible pairs are deleted. The remaining pairs are taken as true ribs. In cases where one border of a rib is detected by the HT but the opposite border is not, the reasoning program will hypothesize the opposite border. The rib border pairs remaining in the database are taken as true rib borders.

The following rules, which are based on the anatomical knowledge of the chest, are used to select the true rib borders from among the candidate ones:

Rule 1: IF two candidate segments intersect,

THEN delete the segment that has a smaller count in the Hough space.

Two segments, U_i and L_j , are said to intersect if the intersection of the two curves, (x_I, y_I) , satisfies $x_{us} \leq x_I \leq x_{ue}$ and $x_{ls} \leq x_I \leq x_{le}$. This also applies to U_i and U_j , and L_i and L_j .

Rule 2: IF a superior and an inferior segment are approximately parallel,

THEN consider them a rib pair.

Two segments are approximately parallel if D_s^{ij} , D_e^{ij} , D_h^{ij} , and D_v^{ij} are all between a lower and an upper bound determined experimentally

$$0.3W_r \leq D_s^{ij}, D_h^{ij}, D_e^{ij}, D_v^{ij} \leq 2W_r \quad (28)$$

where W_r is the estimated rib width described in Section III-C.

Rule 3: IF a candidate segment does not have a pair,

THEN hypothesize its opposite border and add it to the database.

The candidate segment and the hypothesized border thus form a hypothetical pair. The hypothesized border is assumed to have the same count in the Hough space as the candidate segment.

Rule 4: IF two hypothesized pairs intersect,

THEN delete the pair with a lower confidence level.

The steps used to extract the posterior rib borders are summarized in the following algorithm:

Algorithm HT_RIB: Given a chest radiograph, this algorithm extracts the posterior rib borders.

Input: Chest radiograph image $I[i, j]$ and the thoracic cage boundary.

Output: Posterior rib borders.

Step 1: Obtain image edges and select the constructive edge pixels for HT mapping as shown in Fig. 6.

Step 2: Substitute each constructive edge pixel (x, y) into relation (18) and increment by one each array element (a, b, y_c) of the Hough space that satisfies (18). Then, project the 3-D Hough space into 1-D array $K[y_c]$.

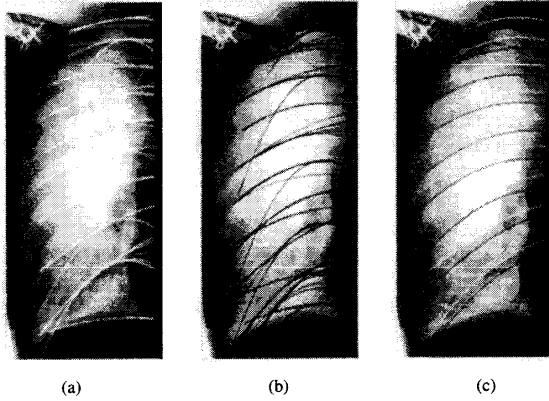


Fig. 8. The candidate and the true rib borders. (a) The superior candidates. (b) The inferior candidates. (c) Extracted true rib borders.

Step 3: Detect the local peaks of the 1-D array and from the peaks determine the candidate rib borders.

Step 4: Apply rule-based reasoning to the candidate rib borders to select potential rib borders.

Lateral rib segments are detected using a similar algorithm. Fig. 8 shows the candidate and final rib borders extracted by the HT and rule-based reasoning. The inferior border of the 10th rib was not detected because of its faint appearance. It was hypothesized to have the same shape as the superior border but translated in the vertical direction by a rib width.

It is possible that the lateral and posterior rib segments determined in this manner do not join smoothly. In the following, an active contour model is described which smoothly joins the lateral and posterior segments of a rib and also repositions pixels on extracted parabolic segments to reconstruct local details in ribs.

IV. LOCALIZATION OF RIB BORDERS

The rib borders extracted using the knowledge-based Hough transform are regarded as approximations to actual rib borders. The approximate rib borders have to be localized to determine the actual shapes of the ribs. To achieve this, a parametric snake [22] is placed along an approximate rib border and is allowed to move in its neighborhood and change its shape. The snake will dynamically minimize its energy while stabilizing. The final position of the snake is taken to be the actual rib border.

A. Snakes

Kass *et al.* [22] introduced energy-minimizing curves known as *snakes* for detecting lines and curves in an image. The snake is an active contour model which constantly minimizes an energy functional. The energy functional consists of both the internal and external energy. The internal energy serves to impose continuity and smoothness constraint on the shape of the snake, and the external energy tends to pull the snake toward salient image features such as image edges. Represent-

ing the snake by a parametric curve $\mathbf{v}(s) = [x(s), y(s)]$, we can write the energy functional by

$$E_{\text{snake}} \equiv \int_0^1 E_{\text{snake}}(\mathbf{v}(s)) ds = \int_0^1 [E_{\text{int}}(\mathbf{v}(s)) + E_{\text{ext}}(\mathbf{v}(s))] ds \quad (29)$$

where E_{int} represents the internal energy, and E_{ext} represents the external energy of the snake.

The internal energy is comprised of a first- and second-order term

$$E_{\text{int}}(\mathbf{v}(s)) = \alpha(s)|\mathbf{v}_s(s)|^2 + \beta(s)|\mathbf{v}_{ss}(s)|^2. \quad (30)$$

The external energy is defined by image forces and external constraints

$$E_{\text{ext}}(\mathbf{v}(s)) = E_{\text{image}}(\mathbf{v}(s)) + E_{\text{con}}(\mathbf{v}(s)). \quad (31)$$

E_{image} is the image energy introduced by various image features such as edges, lines, and terminations. E_{con} is the external constraint defined by the user.

Amini *et al.* [23] proposed a dynamic programming algorithm for minimizing this energy functional. A greedy algorithm was also used for this purpose by Williams *et al.* [24]. Since a snake has to be discretized in a digital image, these algorithms used the following digital terms to estimate the differential terms:

$$\left| \frac{d\mathbf{v}_i}{ds} \right|^2 \approx |\mathbf{v}_i - \mathbf{v}_{i-1}|^2 \quad (32)$$

$$\left| \frac{d^2\mathbf{v}_i}{ds^2} \right|^2 \approx |\mathbf{v}_{i-1} - 2\mathbf{v}_i + \mathbf{v}_{i+1}|^2 \quad (33)$$

where $\mathbf{v}_i = (x_i, y_i)$ is a snake point.

These terms, however, could involve inaccuracies. Equation (32) makes the snake act like an elastic membrane and may cause it to bunch up as it minimizes its energy. When a snake is not closed, it may shrink to a point while minimizing its energy. The second term in (30) is a curvature measure and reflects the smoothness of the curve. Equation (33) also involves inaccuracies. Errors in estimation of the derivatives may be serious enough to displace a snake and miss the actual rib border. In the following, an improved expression for the evaluation of the internal energy terms is proposed. The key idea is to fit a differentiable parametric curve to the discrete snake points and obtain the first- and second-order terms from that curve.

B. Estimation of the Snake Parameters

To accurately estimate the first- and second-order terms in (30), a rational Gaussian (RaG) curve [25] is fitted to the snake points. A RaG curve is defined by

$$\mathbf{v}(s) = \sum_{i=1}^N \mathbf{C}_i g_i(s), \quad 0 \leq s \leq 1 \quad (34)$$

where $\mathbf{C}_i = (x_i, y_i)$ is the i th snake point, $\mathbf{v}(s) = [x(s), y(s)]$, and $g_i(s)$ is its i th basis function defined by

$$g_i(s) = \frac{W_i G_i(s)}{\sum_{j=1}^n W_j G_j(s)}. \quad (35)$$

W_i is the weight associated with the i th point and $G_i(s)$ is a Gaussian of height one

$$G_i(s) = \exp \left\{ -\frac{(s - s_i)^2}{2\sigma_i} \right\}. \quad (36)$$

s_i is the parameter value at which the i th basis function is centered. This parameter is usually not given and has to be estimated from the given points. In this work, we chose $s_i = (i-1)/(N-1)$, $i = 1, \dots, N$, in order to uniformly space the basis functions of the curve. σ_i is the standard deviation of the i th Gaussian and determines the amount of smoothing to be applied to the i th point and points in its neighborhood.

Because curve fitting using RaG does not require solving a system of equations, it is fast. A RaG curve allows weights to be associated with the given points to reflect the relative importance of the points in defining a curve. We used the gradient magnitude of a point as its weight.

Using (34), we can obtain the first-order term of (30) from

$$|\mathbf{v}_s(s)|^2 = \left[\frac{dx(s)}{ds} \right]^2 + \left[\frac{dy(s)}{ds} \right]^2 \quad (37)$$

$$= \left[\sum_{i=1}^N x_i \frac{dg_i(s)}{ds} \right]^2 + \left[\sum_{i=1}^N y_i \frac{dg_i(s)}{ds} \right]^2 \quad (38)$$

where

$$\begin{aligned} \frac{dg_i(s)}{ds} &= W_i G_i(s) \sum_{j=1}^N W_j G_j(s) \\ &\times \left(\frac{s - s_j}{\sigma_j} - \frac{s - s_i}{\sigma_i} \right) \bigg/ \left[\sum_{j=1}^N W_j G_j(s) \right]^2. \end{aligned} \quad (39)$$

Similarly, we obtain the second-order term of (30) from

$$|\mathbf{v}_{ss}(s)|^2 = \left[\frac{d^2x(s)}{ds^2} \right]^2 + \left[\frac{d^2y(s)}{ds^2} \right]^2 \quad (40)$$

$$= \left[\sum_{i=1}^N x_i \frac{d^2g_i(s)}{ds^2} \right]^2 + \left[\sum_{i=1}^N y_i \frac{d^2g_i(s)}{ds^2} \right]^2 \quad (41)$$

where

$$\frac{d^2g_i(s)}{ds^2} = W_i [A(s)B(s) + C(s)D(s)] / A^3(s)$$

$$A(s) = \sum_{j=1}^N W_j G_j(s)$$

$$\begin{aligned} B(s) &= G_i(s) \sum_{j=1}^N W_j G_j(s) \\ &\times \left[\left(\frac{s - s_i}{\sigma_i} \right)^2 - \left(\frac{s - s_j}{\sigma_j} \right)^2 - \frac{1}{\sigma_i} + \frac{1}{\sigma_j} \right] \end{aligned}$$

$$C(s) = 2G_i(s) \sum_{j=1}^N W_j G_j(s) \left(\frac{s - s_j}{\sigma_j} - \frac{s - s_i}{\sigma_i} \right)$$

$$D(s) = \sum_{j=1}^N W_j G_j(s) \left(\frac{s - s_j}{\sigma_j} \right).$$

TABLE I
MEAN AND STANDARD DEVIATION ERRORS IN 10 CHEST RADIOGRAPHS

	rib 2	rib 3	rib 4	rib 5	rib 6	rib 7	rib 8	rib 9	rib 10
mean	0.097	0.085	0.044	0.037	0.038	0.038	0.047	0.16	0.34
standard deviation	0.036	0.029	0.015	0.021	0.014	0.015	0.017	0.18	0.27

The image energy $E_{\text{image}}(x, y)$ is determined such that a snake is pulled toward the edge. The commonly used expression of $E_{\text{image}}(x, y)$ for detection of edges is $E_{\text{image}}(x, y) = -|\nabla I(x, y)|^2$ [23]. This formulation lets an edge with a higher gradient magnitude have a smaller E_{image} . Another expression for $E_{\text{image}}(x, y)$ is based on the zero crossings of the image [22]. E_{image} is defined as $E_{\text{image}}(x, y) = |\nabla^2 G(x, y) \otimes I(x, y)|$, where $G(x, y)$ is a Gaussian used to obtain the zero crossings and \otimes denotes convolution. This expression was based on the idea that edges are zero crossings of the second derivative of an image; therefore, the edges form local minima of $E_{\text{image}}(x, y)$. It makes a snake that is in the neighborhood of an edge contour to gradually move toward the edge. A snake, however, may get trapped in a homogeneous region which also has zero value of E_{image} defined by $|\nabla^2 G(x, y) \otimes I(x, y)|$.

In this work, we determine E_{image} by following the concept of electric potential energy of an electric charge. Each edge pixel is treated as an electric charge, and the image energy is considered as the contribution from all the electric charges. The electric potential energy at (x, y) generated by a unit electric charge at (x', y') , denoted by $P(x, x'; y, y')$, is defined by

$$P(x, x'; y, y') = -\frac{1}{r} = -\frac{1}{\sqrt{(x - x')^2 + (y - y')^2}}. \quad (42)$$

Letting the gradient magnitude of a pixel represent the magnitude of the electric charge at the pixel, we can obtain the image energy field from

$$E_{\text{image}}(x, y) = - \left| \iint \nabla I(x', y') P(x, x'; y, y') dx' dy' \right|. \quad (43)$$

This expression is basically a convolution of $P(x, 0; y, 0)$ with the gradient of the image

$$\begin{aligned} E_{\text{image}}(x, y) &= -|\nabla I(x, y) \otimes P(x, 0; y, 0)| \\ &= -|I(x, y) \otimes \nabla P(x, 0; y, 0)| \end{aligned} \quad (44)$$

where \otimes shows convolution. $E_{\text{image}}(x, y)$ represents the negative average of gradients in a local neighborhood centered at (x, y) . $E_{\text{image}}(x, y)$ will show a low value at or near an edge and a high value at homogeneous areas. Since we allow a curve to freely move and change its shape, no external constraint energy E_{con} is considered.

To localize the rib borders, a greedy algorithm which is similar to that proposed by Williams *et al.* [24] is used. The energy functional is computed at a snake point and each of

its eight neighbors. The location having the smallest value is chosen as the new position of the snake point. The snake points are finally fit to a RaG curve to represent the rib borders. The following algorithm summarizes the steps of the algorithm for localizing the rib borders in a chest radiograph:

Algorithm FINAL_RIB: Given an initialized snake, this algorithm localizes the snake to a rib border.

Input: Initial snake points, $\mathbf{v}(x_i, y_i)$, $1 \leq i \leq N$.

Output: Localized snake, $\mathbf{v}(s) = [x(s), y(s)]$, $0 \leq s \leq 1$.

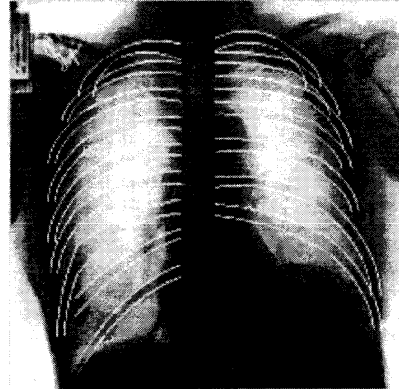
Step 1: Obtain $E_{\text{image}}(x, y)$ from (44).

Step 2: For each snake point i , compute the energy for its current location and each of its eight neighbors.

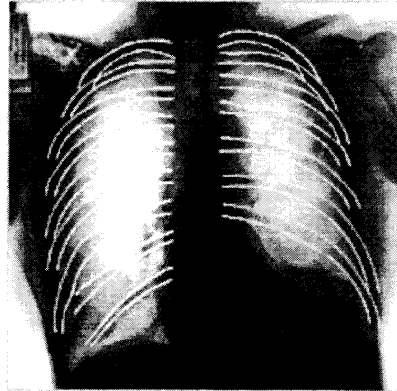
Step 3: Move the snake point to the location having the smallest energy.

Step 4: If no snake point moves, then go to Step 5. Otherwise, go to Step 2.

Step 5: Substitute the final coordinates of the snake points into the equations of the RaG curve to obtain the rib border.



(a)



(b)

Fig. 9. (a) Approximate rib borders consisting of the posterior and lateral segments. (b) The final rib borders.

V. RESULTS

Results of the above algorithm on 10 chest radiographs are shown in Table I. Nine of the radiographs were from adult men and women with healthy ribs. One radiograph was from a patient with a broken rib. The radiographs were of size 512×512 pixels with 256 gray levels.

Fig. 9(a) shows initial rib borders of Fig. 3, and Fig. 9(b) shows the final rib borders determined by the proposed algorithm. The right eighth rib contains a high curvature area indicating a rib fracture. Fig. 10 shows detected rib borders in a radiograph from a healthy individual.

To measure the rib detection accuracy of the proposed algorithm, we asked a radiologist to carefully trace the rib borders on the chest radiographs with a mouse device. Using the obtained result as a standard, we then measured the rib detection error for the i th rib by (45), shown at the bottom of the page, where XOR denotes point-by-point exclusive-or. Corresponding end points of the superior and inferior borders of a rib were joined to form a region. Pixels inside the region were set to one while all other pixels in the image were set to zero. The denominator of (45), therefore, shows the number of pixels in the area corresponding to the i th rib determined manually. The numerator of (45) shows the number of ones obtained when exclusive-oring areas corresponding to the i th rib, pixel-by-pixel, determined manually and by our algorithm. The mean and standard deviation rib detection errors in the 10 chest radiographs are shown in Table I. In many radiographs, parts of the ninth and tenth ribs were missed by the algorithm because of the reduced image contrast generated by the high-voltage imaging technique and confusion due to the shadow of the diaphragm and the abdomen. Errors on the first two

ribs are also high because they overlap with one another and with the clavicles.

The rib detection and localization algorithm was tested on a Sun Sparcstation 1+. Ten seconds were required to extract the thoracic cage boundaries, seven minutes were required to detect the approximate rib borders, and eleven minutes were required to localize the rib borders in chest radiographs of size 512×512 pixels. The localization process took the most time because of its iterative nature.

$$\varepsilon_i = \frac{\text{XOR of the } i\text{th rib areas determined by the radiologist and our algorithm}}{i\text{th rib area determined by the radiologist.}} \quad (45)$$

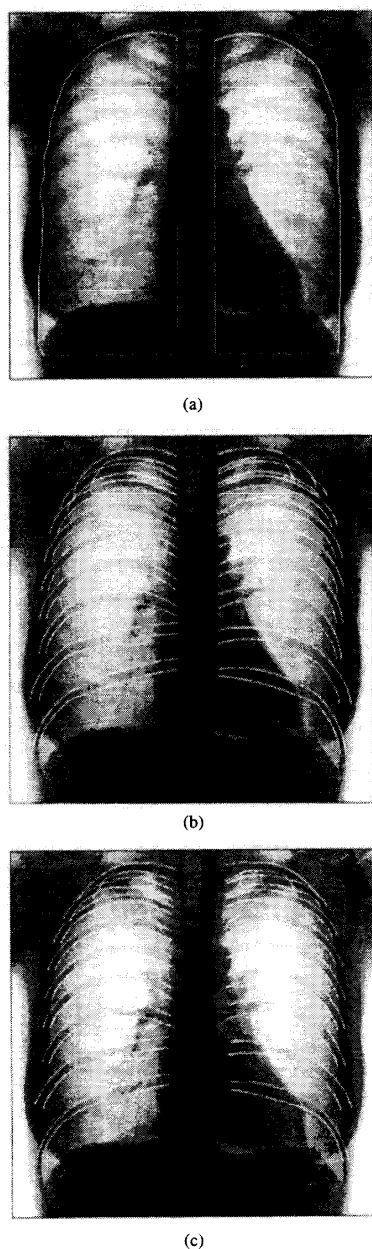


Fig. 10. (a) Isolated rib cage. (b) Approximate rib borders. (c) Final rib borders.

VI. DISCUSSION AND CONCLUSION

An algorithm for detection of posterior rib borders in chest radiographs was presented. The algorithm first isolates the thoracic cage to restrict the area of search for the ribs. It then detects the rib borders using a knowledge-based Hough transform and rule-based reasoning. The rib borders detected by the Hough transform are regarded as approximates and are

localized using parametric snakes. Rational Gaussian curves were used to accurately evaluate the internal energies of snakes. Experimental results show that the knowledge-based HT performs well even when rib borders have very low contrasts. The proposed method has the unique ability to reconstruct local shape details in ribs, enabling detection of abnormalities such as fractures and tumors.

Determination of the approximate rib borders was the most difficult part of the algorithm, primarily due to the weak edge features of ribs and large amounts of noise in chest radiographs. Signal-based edge detectors alone cannot extract the rib borders from noisy chest radiographs. Therefore, rule-based reasoning was used to distinguish false ribs from true ones. The local peaks in the accumulator array usually give rise to candidate rib borders, some of which are wrong. Determining the true rib borders from the candidates is a necessary process in radiographs with faint ribs. Souza [12] and Li *et al.* [11] took vertical sections on a chest radiograph and found rib edge points based on 1-D signal processing. Their methods of rib detection lacked anatomical knowledge of ribs, and consequently failed on chest radiographs of poor quality. In contrast, our symbolic representation of rib borders by parabolic segments enabled application of anatomical knowledge to the rib borders and detection of even very faint rib borders.

Localization of rib borders was accomplished using parametric snakes. Although the positions of some approximate rib borders are very close to the actual ones, the localization step is needed to reconstruct local details in ribs. Experimental results have shown that for most normal ribs, the approximate and localized rib borders are very close. For ribs with local deformations, however, the approximate and localized rib borders are considerably different. The localization process can reveal local shape information that is critical in diagnosis.

The proposed algorithm uses anatomic knowledge to find ribs in a chest radiograph. Some of the anatomic information, such as the rib and spinal column widths, was estimated directly from a given image. Some error is anticipated in estimation of these parameters. Therefore, the algorithm was designed to tolerate the errors by transforming each estimated value into a conservative range of values from which the thoracic cage boundary and the rib borders can be safely determined.

In comparison with previous algorithms for rib detection [6], [8], [9], [12], the proposed method provided the following improvements: 1) More posterior rib borders are located. Eighteen rib borders can be located, including ribs two and ten which are very difficult to find. 2) Rib borders, especially the parts near the thoracic cage boundary, are more accurately localized. This is attributed to the use of rib models in the proposed algorithm. 3) Rib borders with irregularities can be obtained; earlier work could not detect irregularities in ribs. 4) Few constraints are imposed on the input chest radiograph, as it is required only that the patient be in the upright position when taking the radiograph. Translation of the thorax in a chest radiograph is allowed as long as the entire thorax remains in the radiograph.

ACKNOWLEDGMENT

The authors would like to thank Dr. J. Charters, a musculoskeletal radiologist at Rush-Presbyterian-St. Luke's Medical Center, for his contributions to this paper. The authors also would like to thank the reviewers for their insightful comments and suggestions.

REFERENCES

- [1] L. Sider, Ed., *Introduction to Diagnostic Imaging*. New York: Churchill Livingstone, 1986.
- [2] C. B. Rabin and M. G. Baron, *Radiology of the Chest*. Baltimore, MD: Waverly, 1980.
- [3] H. W. Wahner, "Role of bone scanning," in *Diagnosis and Management of Metastatic Bone Disease: A Multidisciplinary Approach*, F. H. Sim, Ed. New York: Raven, 1988, pp. 51-67.
- [4] D. L. Citrin, C. Hougen, W. Zweibel, S. Schlise, B. Pruitt, W. Ershler, T. E. Davis, B. S. Harberg, and A. I. Cohen, "The use of serial bone scans in assessing response of bone metastases to systematic treatment," *Cancer*, vol. 47, pp. 680-685, 1981.
- [5] D. H. Ballard, *Hierarchical Recognition of Tumors in Chest Radiographs with Computer*. New York: Birkhauser Verlag, 1976.
- [6] H. Wechsler, *Automatic Detection of Rib Contours in Chest Radiographs*. New York: Birkhauser Verlag, 1977.
- [7] K. Abe, K. Doi, H. MacMahon, S. Katsuragawa, M. L. Giger, and T. Yanaagisawa, "Analysis of results in a large clinical series of computer-aided diagnosis in chest radiology," in *Proc. Int. Symp. Comput. Assisted Radiology*, 1993, pp. 600-605.
- [8] J. Toriwaki, Y. Suenaga, T. Negoro, and T. Fukumura, "Pattern recognition of chest X-ray images," in *Proc. 1st Int. Joint Conf. Pattern Recognition*, 1973, pp. 125-137.
- [9] E. Persoon, "A new edge detection algorithm and its applications in picture processing," *Comput. Graphics Image Processing*, vol. 5, pp. 425-446, 1976.
- [10] J. H. Kulick and C. M. Brace, "Automatic rib detection in chest radiographs," in *Proc. Int. Joint Conf. Artificial Intell.*, 1978, pp. 697-698.
- [11] C. C. Li and C. P. Fong, "Extraction of dorsal rib contours in chest radiographs by parallel-type processing," in *Proc. Int. Comput. Symp.*, vol. 1, pp. 705-712, 1978.
- [12] P. de Souza, "Automatic detection of ribs in chest radiographs," *Comput. Vision, Graphics Image Processing*, vol. 23, pp. 129-161, 1983.
- [13] K. S. Fu, Y. P. Chien, and E. Persoon, "Computer systems for the analysis of chest X-rays," in *IEEE EASCON*, 1975, pp. 72A-72P.
- [14] D. H. Ballard and C. M. Brown, *Computer Vision*. Englewood Cliffs, NJ: Prentice-Hall, 1982.
- [15] M. Fleck, "Some defects in finite difference edge finders," *IEEE Trans. Pattern Anal. Machine Intell.*, vol. 3, pp. 412-429, 1992.
- [16] J. Illingworth and J. Kittler, "A survey of the Hough Transform," *Comput. Vision, Graphics Image Processing*, vol. 44, pp. 87-116, 1988.
- [17] D. Casasent and R. Krishnapuram, "Curved object location by Hough Transformations and inversion," *Pattern Recognition*, vol. 20, no. 2, pp. 181-188, 1987.
- [18] L. Xu, E. Oja, and P. Kultanen, "A new curve detection method: Randomized Hough Transform (RHT)," *Pattern Recognition Lett.*, pp. 331-339, May 1990.
- [19] R. K. K. Yip, P. K. S. Tam, and D. N. K. Leung, "Modification of Hough Transform for circles and ellipses detection using a 2-dimensional array," *Pattern Recognition*, vol. 25, no. 9, pp. 1007-1022, 1992.
- [20] R. O. Duda and P. E. Hart, "Use of the Hough Transform to detect lines and curves in pictures," *Commun. ACM*, vol. 15, no. 1, pp. 11-15, Jan. 1972.
- [21] S. R. Deans, "Hough Transform from the radon transform," *IEEE Trans. Pattern Anal. Machine Intell.*, vol. PAMI-3, pp. 185-188, 1981.
- [22] M. Kass, A. Witkin, and D. Terzopoulos, "Snakes: Active contour models," *Int. J. Comput. Vision*, pp. 321-331, 1988.
- [23] A. A. Amini, S. Tehrani, and T. E. Weymouth, "Using dynamic programming for minimizing the energy of active contours in the presence of hard constraints," in *Proc. 2nd Int. Conf. Comput. Vision*, 1988, pp. 95-99.
- [24] D. J. Williams and M. Shah, "A fast algorithm for active contours," in *Proc. 3rd Int. Conf. Comput. Vision*, 1990, pp. 592-595.
- [25] A. Goshtasby, "Design and recovery of 2-D and 3-D shapes using rational Gaussian curves and surfaces," *Int. J. Comput. Vision*, vol. 10, no. 3, pp. 233-256, 1993.